PHYSICAL REVIEW E **94**, 020901(R) (2016)

Coupled Leidenfrost states as a monodisperse granular clock

Rui Liu,[*] Mingcheng Yang, Ke Chen,[†] and Meiying Hou[‡]
Beijing National Laboratory for Condensed Matter Physics and CAS Key Laboratory of Soft Matter Physics, Institute of Physics, Chinese Academy of Sciences, Beijing 100190

Kiwing To[§]
Institute of Physics, Academia Sinica, Taipei 115

(Received 11 January 2016; revised manuscript received 31 March 2016; published 23 August 2016)

Using an event-driven molecular dynamics simulation, we show that simple monodisperse granular beads confined in coupled columns may oscillate as a different type of granular clock. To trigger this oscillation, the system needs to be driven against gravity into a density-inverted state, with a high-density clustering phase supported from below by a gaslike low-density phase (Leidenfrost effect) in each column. Our analysis reveals that the density-inverted structure and the relaxation dynamics between the phases can amplify any small asymmetry between the columns, and lead to a giant oscillation. The oscillation occurs only for an intermediate range of the coupling strength, and the corresponding phase diagram can be universally described with a characteristic height of the density-inverted structure. A minimal two-phase model is proposed and a linear stability analysis shows that the triggering mechanism of the oscillation can be explained as a switchable two-parameter Andronov-Hopf bifurcation. Numerical solutions of the model also reproduce similar oscillatory dynamics to the simulation results.

DOI: 10.1103/PhysRevE.94.020901

Nonequilibrium systems may exhibit self-sustained oscillations [1], which play important roles in the generation of periodic rhythms in nature, especially in biological systems [2]. The oscillations in such systems are collective behaviors of many coupled elements, and how to generate spontaneous oscillations through simple couplings is a core problem in understanding these emergent behaviors. Coupled dynamics usually rely on purposely designed frustrations or unidirectional coupling mechanisms to produce stable limit-cycle oscillations [3–6]. The recently discovered granular clock [7–14], which shows that bidiperse beads can oscillate horizontally between connected compartments under vertical vibrations, provides a physical and macroscopic oscillation model without the above constraints. However, the granular clock is triggered by controlling the energy-dependent spatial distributions of the binary beads rather than tuning the coupling of the system, which thus sheds little light on coupling-induced phenomena.

In this Rapid Communication, we numerically show that density heterogeneity, instead of bidispersity, can drive a simple monodisperse granular system to oscillate in coupled columns. The coupling strength of the system can be monotonically tuned, and the oscillation is triggered by the coupling strength, giving a completely different type of granular clock. We find that the oscillation occurs only for an intermediate range of the coupling strength, and an oscillation phase diagram is mapped out for different total numbers of beads and vibrational strengths. A scaling relation for the phase diagram is also found, which indicates that the occurrence of the oscillation depends critically on some structural matching relations of the system. Based on these results, a minimal two-phase model is proposed. A linear stability analysis and numerical solutions of the model qualitatively explain the triggering mechanism and the global dynamics of the oscillation.

Using an event-driven molecular dynamics method [15,16], we simulate vertically vibrated two-dimensional columns of monodisperse spherical beads under gravity (in the y direction), as shown in Fig. 1. In our simulation, the mass m and the diameter d of the beads are both set to 1, and the time unit is $\sqrt{d/g}$, with g being the gravitational acceleration. The width of each column is $W = 10$ [17], and the height of the sidewalls is considered to be infinite. By assuming a sawtooth vibration with infinitely small amplitude A and infinitely large frequency f, the bottom plate is assigned an constant upward velocity $v_b = Af$ but is effectively kept stationary [18]. The coefficient of restitution between the beads is $e = 0.9$, and the dissipation in a particle-wall collision is neglected. Typically, a two-column system is simulated, and the columns are coupled through a bottom window with tunable height h_w in the separation wall [Fig. 1(c)]. The particles are permitted to pass through the window if h_w is large enough.

Initially, each column is filled with an equal number of beads, namely, $N_1(0) = N_2(0) = N/2$ (subscript from 1 to 2 denotes the column index from left to right), with $N = N_1 + N_2$ being the total number. Each simulation runs with the window closed ($h_w = 0$) at the beginning. For proper N and v_b, each column may exhibit a Leidenfrost phenomenon [19,20], i.e., the formation of a density-inverted structure with a high-density clustering phase (CP) supported from below by a gaslike low-density phase (GP) [Fig. 1(a)]. The floating cluster in an uncoupled column may fluctuate as a piston [21] or show noisy resonances [22]. A similar irregular motion has also been observed in our simulation, as shown in Fig. 1(b). However, the irregular motion is relatively small, and the system can still be considered to be in a steady state. In this equally partitioned

[*]lr@iphy.ac.cn
[†]kechen@iphy.ac.cn
[‡]mayhou@iphy.ac.cn
[§]ericto@gate.sinica.edu.tw

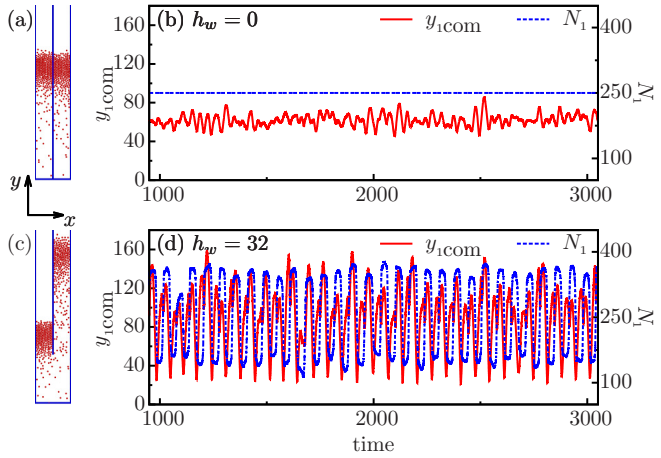

FIG. 1. Simulation results for $N = 500$ and $v_b = 24$: (a) Uncoupled granular columns with $h_w = 0$; (b) the height of the center of mass (y_{1com}) and the number of beads (N_1) for the left column in (a); (c) two coupled granular columns with $h_w = 32$; (d) y_{1com} and N_1 for the left column in (c).

steady state (EPSS), the two columns are statistically identical, and share the same vertical number-density profile $n^0(y)$ with the same characteristic height h_{inv} of the floating cluster. Here, $n^0(y)$ is measured by counting the number of beads (averaged over time) per unit length in the y direction, and h_{inv} is evaluated as the height corresponding to the maximum vertical gradient of $n^0(y)$ [20]. After the EPSS is reached, the window is opened to the preset height of h_w. For two coupled columns with a proper h_w [Figs. 1(c) and 1(d)], we find that the system oscillates fiercely with an amplitude several times larger than that of the fluctuations in the uncoupled case.

For given N and v_b, regular oscillations are observed only for an intermediate range of h_w. As illustrated in Figs. 2(a)–2(c), a good oscillation is observed at $h_w = 58$ for $N = 500$ and $v_b = 30$, but only a fluctuationlike behavior is observed at smaller $h_w = 12$ or larger $h_w = 90$. Generally, a

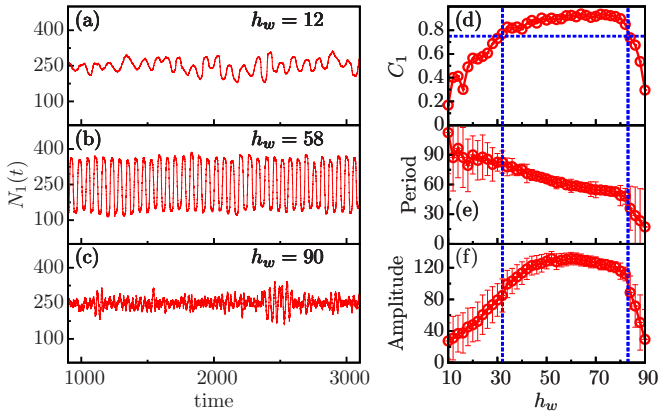

FIG. 2. Coupled dynamics for $N = 500$, $v_b = 30$: $N_1(t)$ for weak coupling at $h_w = 12$ (a), moderate coupling at $h_w = 58$ (b), and strong coupling at $h_w = 90$ (c); (d) the first positive peak value C_1 of the autocorrelation function of $s_1(t)$; the averaged period (e) and amplitude (f) of $s_1(t)$ for different h_w, respectively, with relative error bars in arbitrary units.

larger h_w indicates a stronger coupling between the columns, and the oscillation occurs only in the intermediate coupling regime. To investigate the coupling effect in triggering the oscillation, we have performed simulation runs with different h_w for different N and v_b. Each run results in a curve such as that shown in Figs. 2(a)–2(c). We quantify the quality of the oscillation by calculating the autocorrelation function of $s_i(t) \equiv N_i(t) - N/2$ for each curve,

$$C(\tau) = \langle s_i(t) s_i(t+\tau) \rangle / \sigma^2, \tag{1}$$

where σ is the standard deviation of $s_i(t)$, τ is the time lag, and $\langle \cdot \rangle$ denotes a time average. $C(\tau)$ oscillates for perfect oscillations but quickly vanishes for pure fluctuations. We use the first positive peak value C_1 of $C(\tau > 0)$ to define the quality of an oscillation. For $N = 500$ and $v_b = 30$, C_1 as a function of h_w is shown in Fig. 2(d). C_1 first increases and then decreases, with increasing h_w. At about $h_w = 60$, C_1 reaches its maximum of almost 1 for a nearly perfect oscillation. Empirically, we define an acceptable oscillation with $C_1 \geqslant 0.75$ (above the dotted horizontal line). This gives a lower boundary $h_{LO} = 32$ and a upper boundary $h_{HI} = 82$ (dotted vertical lines) of the range of h_w for acceptable oscillations.

Meanwhile, we perform a Hilbert spectral analysis [2] on each oscillatory curve, which unambiguously gives the instantaneous phase $\phi(t) \in [0, 2\pi)$ and amplitude $A(t)$ of the curve regardless of the oscillation quality,

$$s_i(t) + \mathbf{i}\mathcal{H}[s_i(t)] \equiv A_i(t) \exp[\mathbf{i}\phi_i(t)], \tag{2}$$

where $\mathcal{H}[\cdot]$ denotes a Hilbert transform and $\mathbf{i}$ is the imaginary unit. Then, the apparent oscillation period can be measured from $\phi_i(t)$. For $N = 500$ and $v_b = 30$, the averaged period and amplitude are respectively shown in Figs. 2(e) and 2(f). In the regime $C_1 < 0.75$ ($h_w < h_{LO}$ or $h_w > h_{HI}$), which is assumed to be nonoscillatory, the relative errors for both the period and the amplitude are quite large. Actually, neither the period nor the amplitude is well defined in this regime. In the oscillatory regime $C_1 \geqslant 0.75$ ($h_{LO} \leqslant h_w \leqslant h_{HI}$), the period decreases with increasing h_w, while the amplitude behaves similarly to C_1 and reaches a high plateau, which indicates giant oscillations.

With the empirical criterion $C_1 \geqslant 0.75$, an oscillation phase diagram is obtained for different N and v_b, as shown in Fig. 3(a). Obviously, both h_{LO} and h_{HI} increase with increasing v_b but decrease with increasing N, just as h_{inv} of the EPSS behaves. Then a simple idea is to replot the phase diagram for different N and v_b with a single parameter, $h_{inv}(N, v_b)$. Indeed, we obtain a collapsed phase diagram with h_{inv} for different N and v_b, as shown in Fig. 3(b). Thus, systems of different N and v_b but with the same h_{inv} would share the same oscillatory regime $h_{LO} < h_w < h_{HI}$. The fact that h_{LO} and h_{HI} are only functions of h_{inv} suggests that a structural matching between the window (h_w) and the initial density-inverted structure (h_{inv}) may play an important role in the oscillatory phenomenon. Two deductions on this structural matching concept can be made. First, when $h_w \geqslant h_{inv}$, the two columns share the same

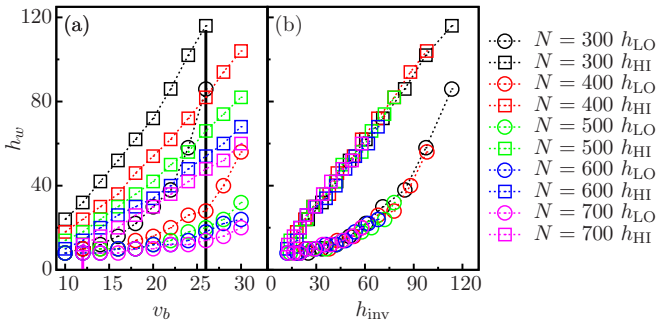

FIG. 3. Oscillation phase diagram: (a) Oscillatory regimes with lower boundaries shown in open circles and upper boundaries in open squares, different N is distinguished by colors, and no oscillation is observed for $N = 700$, $v_b < 12$ and $N = 300$, $v_b > 26$ (marked by vertical solid lines). (b) Collapsed phase diagram in the h_w-$h_{\rm inv}$ plane.

gaseous part, and actually merge into a wider nonoscillatory single column. This explains the collapsed linear relation that $h_{\rm HI} \approx h_{\rm inv}$ in Fig. 3(b). Second, only if h_w corresponds to the height of a large enough vertical gradient of $n^0(y)$, the triggering of the oscillation becomes possible (explained in Fig. 4 and its context). As $n^0(y)$ can be roughly determined by $h_{\rm inv}$ [23], the collapse of $h_{\rm LO}$ in the h_w-$h_{\rm inv}$ plane can be understood. Further side support for the above concept is that no oscillation has been observed for $N = 700$, $v_b < 12$ or $N = 300$, $v_b > 26$. For large $N = 700$ and small $v_b < 12$, $n^0(y)$ is highly compressed due to the strong dissipation. Thus the range from $h_{\rm LO}$ to $h_{\rm HI}$ would be too small to be observed in our simulation. For small $N = 300$ and large $v_b > 26$, the whole system including the floating clusters tends to be gasified. The vertical gradient of $n^0(y)$ would be rather small, even if a density inversion is still present. As we have mentioned above, a small density gradient will not help in triggering an oscillation.

To verify the triggering mechanism of the oscillation, we inspect in detail the oscillatory process. Four time-sequential snapshots of one complete oscillation under $N = 500$, $v_b = 24$, and $h_w = 32$ are shown in Fig. 4. At time $t = 290$, a larger floating cluster is formed in column 1 than that in column 2 because of the excessive population ($N_1 > N_2$). The cluster

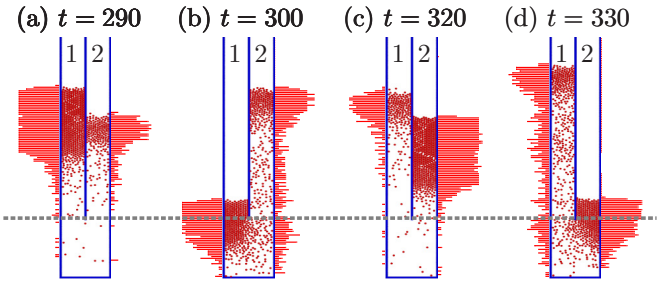

FIG. 4. Time-sequential snapshots with density analysis for one oscillation under $N = 500$, $v_b = 24$, and $h_w = 32$: (a) $t = 290$; (b) $t = 300$; (c) $t = 320$; (d) $t = 330$; instantaneous density profiles are shown in horizontal bars on the left (column 1) or right (column 2) side of each granular column, and the gray dashed line indicates the height of the window.

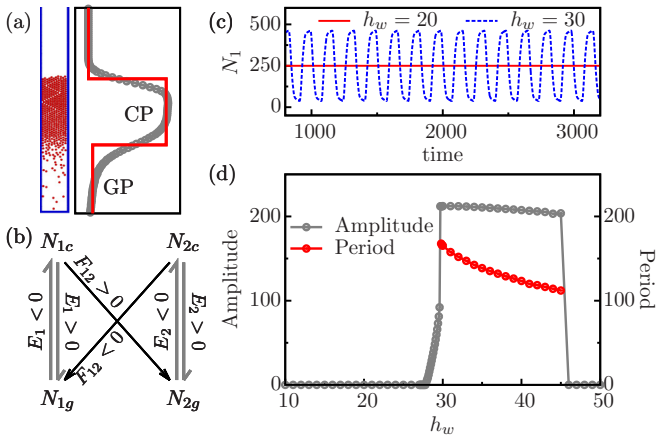

FIG. 5. Theoretical model and numerical solutions for $N = 500$ and $v_b = 24$: (a) The simplified density profile (red line) for a granular column; (b) the net flows between phases considered in our model; (c) $N_1(t)$ for the steady state at $h_w = 20$ and the oscillatory state at $h_w = 30$; (d) oscillation amplitude and period of $N_1(t)$ for different h_w.

in column 1 sinks into the window region due to the lack of enough support at $t = 300$, and there the distinct density difference between the two columns drives a massive flow of beads from column 1 to 2. The beads that have entered column 2 are heated up by the bottom plate, and push the smaller cluster on top to a higher place. As dissipation increases dramatically with the increased population, the beads in column 2 start to condensate and form an even larger cluster at $t = 320$. Meanwhile, a much smaller but higher cluster is formed in column 1 through an evaporation process due to the decreased population. The relaxation time needed by both the evaporation and condensation processes, as well as the large horizontal density difference, allows enough beads to transfer, which maintains a nondamping oscillation. After the evaporation and condensation, the situation becomes similar to that of Fig. 4(a), except that the two columns have been playing reversed roles. Then, following the same process, column 2 drives beads back into 1, as shown in Fig. 4(d). The above oscillation picture is valid even in the triggering moment, when the two columns are almost identical. A large vertical gradient in $n^0(y)$ around h_w may cause a large horizontal density difference in the window region under perturbations. Thus any small population difference between the columns may be amplified through the above process and the oscillation can be triggered.

To confirm the theoretical feasibility of the structural matching concept and to clarify the critical role played by the density gradient, we propose a minimal model for the oscillation. We simplify the density profile $n_i(y)$ of any column i by assuming that both GP and CP, respectively, with a population of N_{ig} and $N_{ic} = N_i - N_{ig}$, are homogeneous [Fig. 5(a)]. Both the intercolumn and the intracolumn (between GP and CP) flows of beads need to be considered. First, the outflow flux from column i can be measured as $F_i = \lambda \int_0^{h_w} n_i(y)dy$ ($\lambda > 0$) [18,24], where λ is a v_b-dependent parameter. The net flux between the columns, $F_{12} = -F_{21} = F_1 - F_2$, should mainly describe the transfer of beads from CP in one column to GP in the other column, as shown in Fig. 4. To emphasize this

point, we further assume constant number densities, n_g and n_c, respectively, for GP and CP. Thus between the columns, only CP-to-GP flows are allowed due to the density difference, as illustrated in Fig. 5(b). Employing the constant-density assumption, F_i can be easily calculated (see the Appendix). Second, we simply describe the flow between GP and CP in column i with a rate $E_i = -\beta(N_{ig} - N_{ig}^s)$ ($\beta > 0$), where superscript s represents the steady state of the column in the uncoupled case, and β is another v_b-dependent parameter. As shown in Fig. 5(b), $E_i > 0$ indicates evaporation and $E_i < 0$ describes condensation. We assume that $N_{ig}^s(N_i) = N_i e^{-\alpha N_i}$ ($\alpha > 0$) [25], with a fitting parameter α. Finally, the dynamics of the system can be described by the following equations,

$$\dot{N}_{ig} = E_i + F_{ji}\mathbf{H}(F_{ji}), \quad \dot{N}_i = \dot{N}_{ic} + \dot{N}_{ig} = F_{ji}, \quad (3)$$

where the overdot denotes the derivative with respect to time, $\mathbf{H}(\cdot)$ is the Heaviside step function, i runs from 1 to 2, and $j = 3 - i$.

When $h_w = 0$, the coupling term $F_{ij} = 0$. For an initial state with $N_1 = N_2 = N/2$, the system represented by Eqs. (3) will obviously stay in an EPSS with fixed $N_{ig} = N_{ig}^s(N/2) \equiv n_g h_{\text{inv}}$. Around the EPSS, $\partial F_{12}/\partial N_{ig} \propto S \equiv \lambda(n_c/n_g - 1)\mathbf{H}(h_w - h_{\text{inv}})$. A linear stability analysis (see the Appendix) shows that an Andronov-Hopf bifurcation with respect to β exists for $S > 0$ but not for $S = 0$. Though β cannot be varied in our case, the system is possibly already in the oscillatory regime ($\beta < S$) once the Andronov-Hopf bifurcation is switched on by S. Thus the triggering dynamics of the oscillation can be understood as a switchable two-parameter Andronov-Hopf bifurcation, and the switch S gives a structural matching boundary $h_{\text{LO}} = h_{\text{inv}}$ for the oscillation. Moreover, $S \propto (n_c - n_g)$, which also indicates the density gradient around the height of h_{inv} should be large enough ($S > \beta$) to trigger the oscillation. Since neither h_w nor S is the Andronov-Hopf bifurcation parameter, it is also explained why no obvious Andronov-Hopf-like triggering behaviors of oscillation amplitudes and periods are found in our simulation results.

To numerically solve the model, a close packing density $n_c = 2/\sqrt{3}W$ for CP and $n_g = 0.2W$ for GP are adopted according to the simulation results. We keep N and v_b fixed, say, $N = 500$, $v_b = 24$. Then, $\alpha \approx 0.006$ can be obtained by fitting the data from the simulation of isolated columns, and this gives $h_{\text{inv}} \approx 27.9$. We choose $\beta = 0.05$, $\lambda = 0.20$ to recover similar dynamics to the simulation results. Then Eqs. (3) can be solved with the Runge-Kutta method. A stable fixed-point solution corresponding to the EPSS exists for $S = 0$ ($h_w < h_{\text{inv}}$), and loses its stability to give way to an oscillation when S becomes positive ($h_w > h_{\text{inv}}$), as shown in Fig. 5(c). Our model also sets an upper boundary $h_{\text{HI}} \approx 45$ for the oscillation. In the oscillatory regime $h_{\text{LO}} < h_w < h_{\text{HI}}$, similar behaviors in the oscillation amplitude and period to the simulation results [Figs. 2(e) and 2(f)] are found, as shown in Fig. 5(d). Hence almost all the characteristics of the oscillation are recovered with this simple model.

In conclusion, a different class of coupling-induced giant oscillations is discovered in a simple monodisperse granular system, which indicates that high-energy spatial patterns such as granular Leidenfrost states may be spontaneously converted into temporal patterns through mere coupling in a nonequilibrium system. The triggering mechanism of the oscillation is confirmed and a switchable Andronov-Hopf bifurcation is identified by our minimal analytical model. Controlled by the switch parameter, the dynamics of the system differs significantly from a typical Andronov-Hopf bifurcation.

Furthermore, the oscillation is robust in simulation for different restitution coefficients e or inelastic collision models, or for a reasonable range of column widths W [26]. Instead of the underlying mechanism of the clustering behavior, the density structure proves to be critical to the oscillation, as also verified by our analytical model. A previous study on a similar system [27] has reported that, in the absence of external fields, clustering behaviors due to dissipation only lead to asymmetric steady states (granular Maxwell demon). In such a circumstance, the density structure barely stores any potential energy and cannot provide an efficient feedback mechanism in the coupled dynamics. Thus no oscillation can be observed. Similar to the phenomena of granular Maxwell demon [28] and the bidisperse granular clock [14], our system can be extended to the case of three or more coupled columns, in which similar oscillations are observed [26]. Due to the simplicity and extensibility of our system, the above results may help in understanding some complex biological oscillations. Our further study will focus on the experimental observation of such a monodisperse granular clock.

We thank Yinchang Li for his preliminary work on the simulation. R.L. thanks C. K. Chan and P. Y. Lai for useful discussions. This work is supported by National Natural Science Foundation of China (Grants No. 11404378 and No. 11474326), the MOST 973 Program (Grant No. 2015CB856800), and the Chinese Academy of Sciences "Strategic Priority Research Program SJ-10" (Grant No. XDA04020200).

APPENDIX: LINEAR STABILITY ANALYSIS

In this Appendix, we provide the details of the linear stability analysis of our theoretical model [Eqs. (3)]. All the analytic calculations and analyses are performed near the triggering point from an EPSS to an oscillatory state, and thus only provide information on the lower instability boundary $h_w = h_{\text{LO}}$.

First, we give an explicit form for the flux function F_{ij} in Eqs. (3). With the constant density assumption for both CP and GP, the outflux F_i from any column i can be simply calculated as

$$F_i = \lambda[n_g h_w + (n_c - n_g)(h_w - h_{ig})\mathbf{H}(h_w - h_{ig})], \quad (A1)$$

where $h_{ig} = N_{ig}/n_g$, and n_c and n_g are, respectively, the linear number densities of CP and GP ($n_c > n_g$).

Since the total number of beads $N = N_1 + N_2$ is conserved, there are only three independent variables in Eqs. (3). By choosing N_{1g}, N_{2g}, and N_1 to be independent, other variables can be calculated as $N_{ic} = N_i - N_{ig}$, $N_2 = N - N_1$. In the EPSS, we have $N_1 = N_2 = N/2$, $N_{ig} = N_{ig}^s(N/2)$,

$N_{ic} = N/2 - N_{ig}^s(N/2)$, $h_{ig} = h_{\rm inv}$, $F_{ij} = 0$, and

$$\frac{\partial E_i}{\partial N_j} = \epsilon_{ij}\beta R, \quad \frac{\partial E_i}{\partial N_{jg}} = -\delta_{ij}\beta, \tag{A2}$$

$$\frac{\partial F_i}{\partial N_j} = 0, \quad \frac{\partial F_i}{\partial N_{jg}} = -\delta_{ij} S, \tag{A3}$$

where $R = (1-\alpha N/2)e^{-\alpha N/2}$, $S = \lambda(n_c/n_g - 1)\mathbf{H}(h_w - h_{\rm inv})$, δ_{ij} is the Kronecker symbol, and $\epsilon_{ij} = 1$ for $i = j$ and $\epsilon_{ij} = -1$ for $i \neq j$.

For small perturbations $\delta N \equiv (\delta N_{1g}, \delta N_{2g}, \delta N_1)$ in (N_{1g}, N_{2g}, N_1) around an EPSS, Eqs. (3) can be linearized. According to Eqs. (A2) and (A3), the Jacobian matrix of the linearized equations of δN reads

$$M = \begin{bmatrix} -\beta + S\mathbf{H}(0) & -S\mathbf{H}(0) & \beta R \\ -S[1-\mathbf{H}(0)] & -\beta + S[1-\mathbf{H}(0)] & -\beta R \\ S & -S & 0 \end{bmatrix}. \tag{A4}$$

The characteristic polynomial of M is

$$\det(tI - M) = (t+\beta)[t^2 + (\beta - S)t - 2\beta RS], \tag{A5}$$

where I is the identity matrix, and all $\mathbf{H}(0)$ terms cancel out. Obviously, the corresponding eigenvalues are

$$t_1 = -\beta,$$

$$t_{2,3} = \frac{-(\beta - S) \pm \sqrt{(\beta - S)^2 + 8\beta RS}}{2}. \tag{A6}$$

In our case, $\alpha = 0.006$, $N = 500$, which gives $R < 0$. $S = 0$ for $h_w < h_{\rm inv}$, and $S > 0$ for $h_w \geqslant h_{\rm inv}$. S can be theoretically negative, by assuming $n_c < n_g$ in the case of a normal gaseous state without density inversion. Suppose $S > 0$. When $\beta = S$, the conjugate pair of eigenvalues $t_{2,3} = \pm\mathbf{i}\sqrt{-8\beta RS}$ are purely imaginary, and the real eigenvalue t_1 is negative. Thus an Andronov-Hopf bifurcation with respect to β arises when β goes from $\beta > S$ (fixed point) to $\beta < S$ (limit cycle). However, only real eigenvalues exist and no limit cycle will appear if $S \leqslant 0$, no matter how β varies. Hence the Andronov-Hopf bifurcation can be switched on or off by setting $S > 0$ or $S \leqslant 0$.

As we choose $\beta = 0.05$, $\lambda = 0.20$, $n_c/n_g \approx 5.77$ in our numerical solution, $\beta < S$ is automatically satisfied and the system is already in the oscillatory regime once the Andronov-Hopf bifurcation is switched on by S (h_w). Essentially, $S > \beta$ indicates that density inversion with a large enough vertical density gradient is a necessary condition for the system to trigger an oscillation.

[1] A. A. Andronov and C. E. Chaikin, *Theory of Oscillations* (Princeton University Press, Princeton, NJ, 1949).

[2] A. Pikovsky, M. Rosenblum, and J. Kurths, *Synchronization: A Universal Concept in Nonlinear Sciences* (Cambridge University Press, New York, 2001).

[3] V. In, A. R. Bulsara, A. Palacios, P. Longhini, A. Kho, and J. D. Neff, Phys. Rev. E **68**, 045102(R) (2003).

[4] V. In, A. Palacios, A. R. Bulsara, P. Longhini, A. Kho, J. D. Neff, S. Baglio, and B. Ando, Phys. Rev. E **73**, 066121 (2006).

[5] A. R. Bulsara, V. In, A. Kho, P. Longhini, A. Palacios, W. J. Rappel, J. Acebron, S. Baglio, and B. Ando, Phys. Rev. E **70**, 036103 (2004).

[6] M. Hernandez, V. In, P. Longhini, A. Palacios, A. Bulsara, and A. Kho, Phys. Lett. A **372**, 4381 (2008).

[7] R. Lambiotte, J. M. Salazar, and L. Brenig, Phys. Lett. A **343**, 224 (2005).

[8] G. Costantinia, D. Paolotti, C. Cattuto, and U. M. B. Marconi, Physica (Amsterdam) **347**, 411 (2005).

[9] T. Miao, Y. Liu, F. Miao, and Q. Mu, Chin. Sci. Bull. **50**, 726 (2005).

[10] S. Viridi, M. Schmick, and M. Markus, Phys. Rev. E **74**, 041301 (2006).

[11] M. Hou, H. Tu, R. Liu, Y. Li, K. Lu, P. Y. Lai, and C. K. Chan, Phys. Rev. Lett. **100**, 068001 (2008).

[12] R. Liu, Y. Li, and M. Hou, Phys. Rev. E **79**, 052301 (2009).

[13] Y. Li, R. Liu, and M. Hou, Phys. Rev. Lett. **109**, 198001 (2012).

[14] S. Hussain, Y. Li, F. Cui, Q. Zhang, E. Pierre, and M. Hou, Chin. Phys. Lett. **29**, 034501 (2012).

[15] D. C. Rapaport, *The Art of Molecular Dynamics Simulation* (Cambridge University Press, Cambridge, U.K., 1997).

[16] T. Pöschel and T. Schwager, *Computational Granular Dynamics: Models and Algorithms* (Springer, Berlin, 2005).

[17] For $W \geqslant 20$, horizontal density symmetry will be broken and convective flows may also appear. Both will make the oscillation unstable. A similar effect in the bidisperse granular clock has been discussed in Q.-Y. Liu, M.-B. Hu, R. Jiang, and Y.-H. Wu, Phys. Rev. E **87**, 014202 (2013).

[18] J. Eggers, Phys. Rev. Lett. **83**, 5322 (1999).

[19] B. Meerson, T. Pöschel, and Y. Bromberg, Phys. Rev. Lett. **91**, 024301 (2003).

[20] P. Eshuis, K. van der Weele, D. van der Meer, and D. Lohse, Phys. Rev. Lett. **95**, 258001 (2005).

[21] J. J. Brey and M. J. Ruiz-Montero, Phys. Rev. E **81**, 021304 (2010).

[22] N. Rivas, S. Luding, and A. R. Thornton, New J. Phys. **15**, 113043 (2013); C. R. K. Windows-Yule, N. Rivas, D. J. Parker, and A. R. Thornton, Phys. Rev. E **90**, 062205 (2014); also, a similar phenomenon under zero gravity: E. Khain and B. Meerson, Europhys. Lett. **65**, 193 (2004).

[23] With nearly a close packing density deep inside CP and a small density approaching zero off the bottom plate in GP, $n^0(y)$ having the same $h_{\rm inv}$ would be quite similar even for different N and v_b.

[24] R. Mikkelsen, D. van der Meer, K. van der Weele, and D. Lohse, Phys. Rev. Lett. **89**, 214301 (2002); Phys. Rev. E **70**, 061307 (2004).

[25] This form reasonably gives $N_{ig}^s \to 0$ for large N_i and $N_{ig}^s \to N_i$ for small N_i in the case of given v_b.

[26] R. Liu *et al.* (unpublished).

[27] J. J. Brey, F. Moreno, R. García-Rojo, and M. J. Ruiz-Montero, Phys. Rev. E **65**, 011305 (2001).

[28] J. J. Brey, R. García-Rojo, F. Moreno, and M. J. Ruiz-Montero, Eur. Phys. J. Spec. Top. **146**, 323 (2007).